CONF-8610135--59

AGING DEGRADATION OF CAST STAINLESS STEEL*

O. K. Chopra and H. M. Chung

Materials and Components Technology Division
Argonne National Laboratory
Argonne, Illinois 60439

CONF-8610135--59

DE87 004939

October 1986

To be presented at the 14th Water Reactor Safety Information Meeting, October 27-31, 1986, National Bureau of Standards, Gaithersburg, MD.

*Work supported by the Office of Nuclear Regulatory Research, U. S. Nuclear Regulatory Commission, under Contract W-31-109-Eng-38.

AGING DEGRADATION OF CAST STAINLESS STEEL

O. K. Chopra and H. M. Chung

Materials and Components Technology Division
Argonne National Laboratory
Argonne, Illinois 60439

Abstract

A program is being conducted to investigate the significance of in-service embrittlement of cast duplex stainless steels under light-water reactor operating conditions. Microstructures of cast materials subjected to long-term aging either in reactor service or in the laboratory have been characterized by TEM, SANS, and APFIM techniques. Two precipitate phases, i.e., the Cr-rich α' and Ni- and Si-rich G phase, have been identified in the ferrite matrix of the aged steels. The results indicate that the low-temperature embrittlement is primarily caused by α' precipitates which form by spinodal decomposition. The relative contribution of G phase to loss of toughness is now known. Microstructural data also indicate that weakening of ferrite/austenite phase boundary by carbide precipitates has a significant effect on the onset and extent of embrittlement of the high-carbon CF-8 and CF-8M grades of stainless steels, particularly after aging at 400 or 450°C. Data from Charpy-impact, tensile, and J-R curve tests for several heats of cast stainless steel aged up to 10,000 h at 350, 400, and 450°C are presented and correlated with the microstructural results. Thermal aging of the steels results in an increase in tensile strength and a decrease in impact energy, J_{IC}, and tearing modulus. The fracture toughness results show good agreement with the Charpy-impact data. The effects of compositional and metallurgical variables on loss of toughness are discussed.

1. Introduction

It has long been known that ferritic stainless steels are susceptible to severe embrittlement when exposed to temperatures in the range of 300 to 500°C, due to precipitation of the chromium-rich α' phase.[1-3] The potential for significant embrittlement of cast duplex stainless steels has been confirmed by recent studies on cast materials that were aged at temperatures between 300 and 450°C for times up to 70,000 h (~8 yr).[4-7] Thermal aging of cast duplex steels at these temperatures causes an increase in hardness and tensile strength and a decrease in ductility, Charpy-impact strength, and J_{IC} fracture toughness of the material. The room-temperature impact energy can be reduced by ~80% after aging for ~8 yr at temperatures as low as 300°C. An increase in ferrite content of the cast structure increases the susceptibility to embrittlement.

Most investigations characterize the degree of embrittlement in terms of Charpy-impact energy in notched toughness tests. The current "best estimates" of the degree of embrittlement at reactor operating temperatures, i.e., 280 to 330°C, are obtained from Arrhenius extrapolations of laboratory data obtained at higher temperatures. The aging time to reach a given degree of embrittlement at different temperatures is determined from

$$t = 10^{P} \exp\left[\frac{Q}{R}\left(\frac{1}{T} - \frac{1}{673}\right)\right], \qquad (1)$$

where Q is the activation energy, R the gas constant, T the absolute temperature, and P the aging parameter which represents the degree of aging reached after 10^{P} h at 400°C. The activation energy for the process of embrittlement has been described as a function of chemical composition of the cast material.[7] Thus,

$$Q(\text{kcal/mole}) = -43.64 + 4.76\ (\%\ Si) + 2.65\ (\%\ Cr) + 3.44\ (\%\ Mo). \quad (2)$$

The activation energy for the process of embrittlement ranges between 15 and 25 kcal/mole for the CF-3, CF-8, and CF-8M grades of cast stainless steels. For a given composition of the cast material, Eqs. (1) and (2) can be used to determine the aging conditions that are representative of reactor service. For a cast material with an activation energy of 24,000 kcal/mole, the end-of-life for cold leg (i.e., 40 yr at 290°C) is equivalent to 10,000 h at 400°C and the end-of-life for hot leg (i.e., 40 yr at 320°C) is equivalent to 30,000 h at 400°C. Consequently, the laboratory data obtained for materials aged at 400°C may be used to predict the end-of-life impact strength of the materials.

Such an approach is a powerful tool for accelerated testing when it can be clearly established that the same mechanisms are operating over the temperature range involved in the extrapolation. Recent studies indicate that the carbon content in the steel is an important factor in controlling the overall process of embrittlement, particularly for aging temperatures $\geq$400°C.[8] At least two processes contribute to the embrittlement of duplex stainless steels, viz., weakening of the ferrite/austenite phase boundary by carbide precipitates, and embrittlement of the ferrite matrix by the formation of additional phases. The former has a significant effect on embrittlement of high-carbon materials, e.g., CF-8 or CF-8M grades. The Charpy-impact data for high-carbon grades of cast steels indicate that the existing correlations do not accurately represent the embrittlement behavior over the temperature range of 300 to 450°C.

Microstructural studies on low-temperature aged cast stainless steel revealed the existence of the G-phase (an fcc phase rich in Ni and Si) and other phases which could not be identified.[8-11] The G-phase and α' phase have been identified by transmission electron microscopy (TEM),[8] atom probe field-ion microscopy (APFIM),[12,13] and by extraction replica techniques.[14] The relative contribution of α' and G phases to low-temperature embrittlement is, however, not known. The Charpy-impact data for aged cast stainless steel yield activation energies well below the 55 kcal/mole value associated with chromium bulk diffusion, the process that has most commonly been assumed to be rate controlling in the low-temperature embrittlement of ferritic steels. These results indicate differences in the mechanism of embrittlement over the temperature range 300 to 450°C.

The objectives of this program are to (1) characterize the microstructure of in-service reactor components and laboratory-aged material, correlate microstructure with loss of fracture toughness, and identify the mechanism of embrittlement; (2) determine the validity of laboratory-induced embrittlement data for predicting the toughness of component materials after long-term aging at reactor operating temperatures; (3) characterize the loss of fracture toughness in terms of fracture mechanics parameters to provide the data needed to assess the safety significance of embrittlement; and (4) provide additional understanding of the effects of key compositional and metallurgical variables on the kinetics and degree of embrittlement.

2. Material Characterization

Material was obtained from nineteen experimental heats (static-cast keel blocks) and six commercial heats (centrifugally cast pipes and static-cast pump impeller and pump casing ring) of CF-3, -8, and -8M grades of cast duplex

stainless steel. Six of the experimental heats were also procured in the form of 76-mm-thick slabs. Charpy-impact specimen blanks were obtained from all heats of material. Blanks for compact tension and tensile specimens were obtained from sections of cast pipes, pump casing ring, pump impeller, and the cast slabs. The specimen blanks are being aged at 450, 400, 350, 320, and 290°C for times up to 50,000 h. Data on the chemical composition, ferrite content, hardness, ferrite morphology, and grain structure of the experimental and commercial heats have been reported earlier.[8-10]

The Cr and Ni equivalent for the various heats are plotted on the modified Schaeffer diagram in Fig. 1. The two-phase regimes covered by the ASTM specification for CF-8 or -3 and CF-8M grades of cast stainless steel are shown by solid and dashed lines, respectively. The chemical compositions of the cast materials used in the Georg Fischer (GF) study,[4] are also included in Fig. 1. The composition and ferrite content of the ANL heats vary over the entire range represented by the ASTM specifications. The cast materials used in the GF study have high ferrite content and the compositions of most of the materials are outside the ASTM specifications. Combined data from the two studies can be used to establish the effects of compositional variables on the embrittlement behavior of cast duplex steels.

Fractured impact test bars from five heats of aged cast stainless steel grades CF-8 and CF-8M were obtained from Georg Fischer Co. (GF), Switzerland, for microstructural characterization. The materials are from a previous study of the long-term aging behavior of cast stainless steel.[4] The specimens were aged for 3000, 10,000, and 70,000 h at 300, 350, and 400°C. A cover plate assembly from the recirculation pump of the KRB reactor was also procured. The boiling-water reactor was in service for ~12 yr. (~8 yr. at service temperature of 284°C).

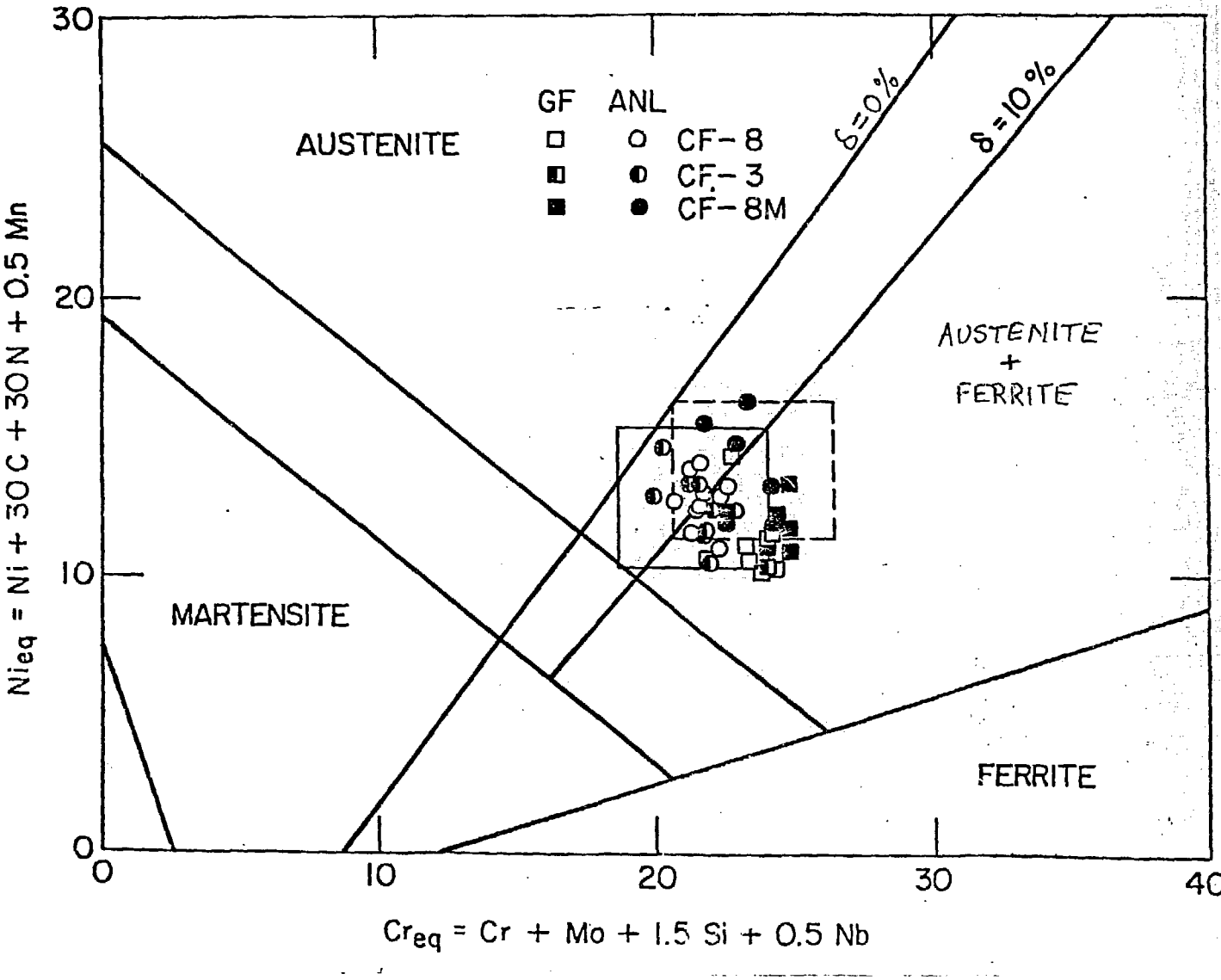

Fig. 1. Schaeffler Diagram and Ferrite Content of Cast Duplex Stainless Steels Used for the Present Study and for the Study by Georg Fischer Company.

3. Microstructural Characterization

In previous reports,[8-11] the microstructures of the laboratory- and reactor-aged cast stainless steel specimens have been characterized primarily by means of transmission and scanning electron microscopies (TEM and SEM). The microstructural characteristics were correlated with the fracture behavior of room-temperature impact specimens to provide a mechanistic interpretation of the aging embrittlement phenomenon. In particular, the mechanistic evaluation was intended to critically examine the validity of the simulation tests of the in-reactor degradation by accelerated laboratory aging at $\gtrsim$400°C, and thereby to evaluate methods of extrapolating the high-temperature test results to the reactor operating temperatures of 280-320°C. Previous results[8-11] indicated that three phases were responsible for the embrittlement of the ferrite phase: Cr-rich α', Ni- and Si-rich G-phase, and unidentified Type-X precipitates. In addition to these phases, precipitates of $M_{23}C_6$ carbides were also identified to form on austenite/ferrite phase boundaries, and the carbide precipitation was found to be associated with the weakening of the phase boundary. The microstructures of low-temperature aged material have now been characterized by small-angle neutron scattering (SANS) and atom-probe field ion microscopy (APFIM) techniques in addition to the TEM examination. Results obtained by the three complimentary techniques have been compared and correlated with the aging histories.

The morphology and electron diffraction characteristics of the Type-X precipitates were analyzed further. The analysis showed that the precipitates are actually G-phase which was preferentially formed on the dislocations during aging at ~300°C. TEM images of precipitates formed on or near dislocations in two GF heats of cast material aged for 70,000 h at 300°C are

shown in Fig. 2. Due to the small volume fracture of the precipitates, only a few very weak reflections could be detected on the selected-area-diffraction (SAD) patterns. A careful examination of several SAD patterns indicated that the weak reflections belong to the G-phase. This is illustrated in a comparison of SAD patterns containing the weak reflections associated with the Type-X phase, Fig. 3a, and the pattern characteristic of G-phase, Fig. 3b. Orientations of the ferrite phase of the two SAD patterns are identical, i.e., (011) zone. The weak reflection denoted by the arrow in Fig. 3a is indeed the relatively strong ($3\bar{3}3$) reflection of the G-phase. The microstructural data indicate that the dislocations act as preferential nucleation sites for G-phase precipitation. Thermal aging for 70,000 h at 300°C produces fine precipitates (~6 nm in size) of G-phase on dislocations whereas at 400°C, the G-phase precipitates on dislocations as well as homogeneously in the ferrite matrix. The size of the G-phase which precipitated on dislocations at 400°C is characteristically larger than those away from the dislocations, i.e., ~15 versus ~5 nm.

Specimens from two GF heats aged at 400°C have been analyzed by SANS technique to provide quantitative information on the size and distribution of precipitates.[15] Monochromatic beams of neutrons of wavelength of 0.475 nm were impinged on the aged specimens and the intensities of the scattered neutrons were measured by a detector as a function of scattering angle. The results indicate that the scattering centers for the analysis are the G-phase precipitates. The size distributions of the precipitates, obtained from the SANS analysis, show that the size of the majority of the precipitates increases from ~1.8 nm for 10,000 h aging to ~5.5 nm for 70,000 h of aging at 400°C. These results are in good agreement with the TEM observations. However, the scattering curves do not indicate a presence of a peak

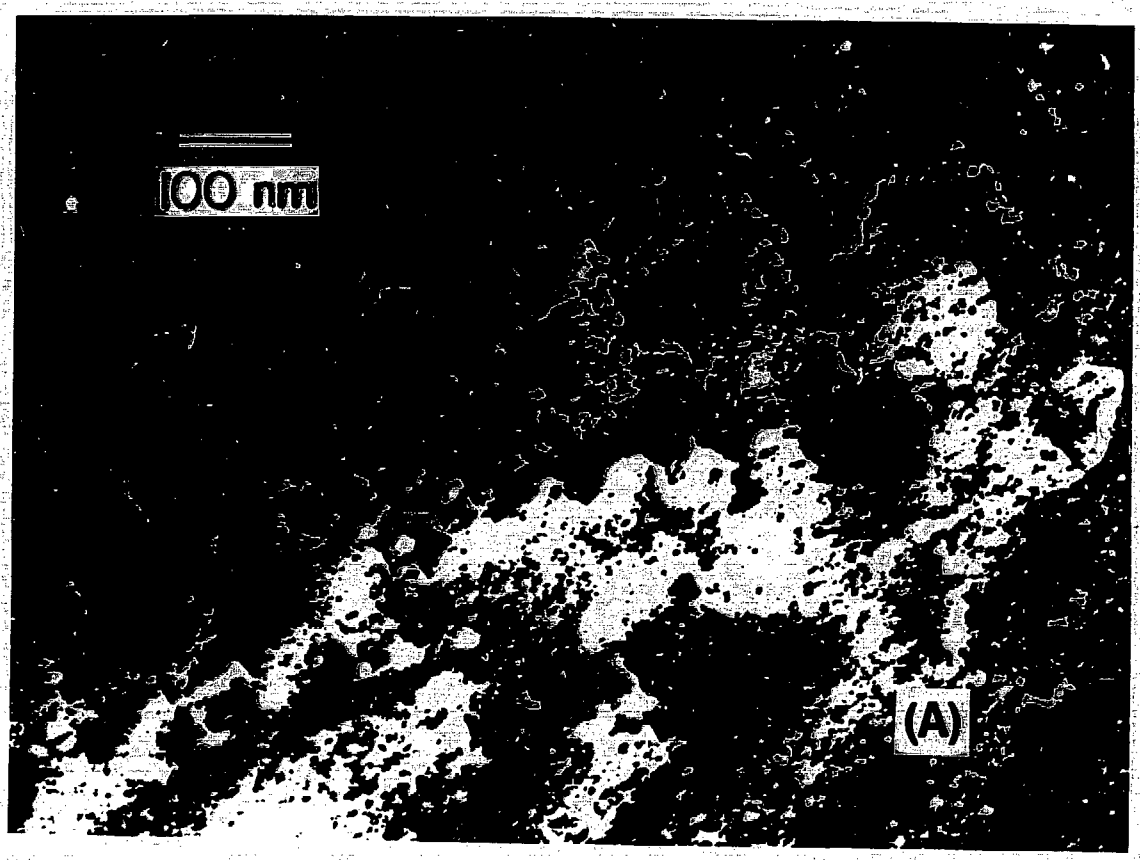

Fig. 2. TEM Images Showing Precipitates Formed on or Near Dislocations During Aging at 300°C for 70,000 h. (A) Dark-field image from superposed reflections of ferrite and the precipitate, heat 278, and (B) bright-field image, heat 280.

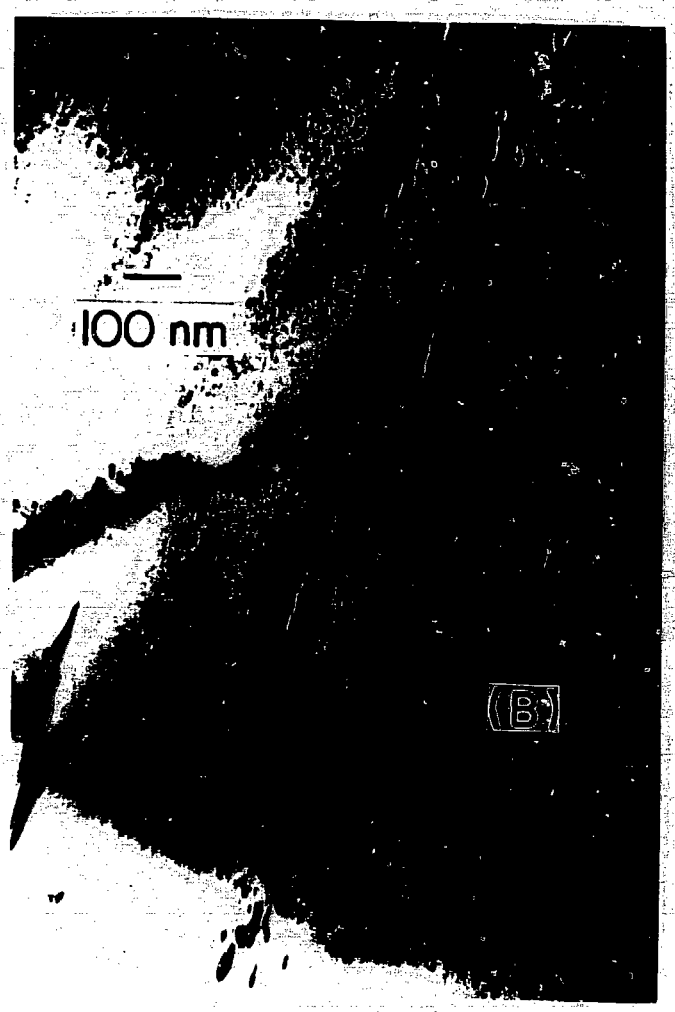

Fig 2(B)

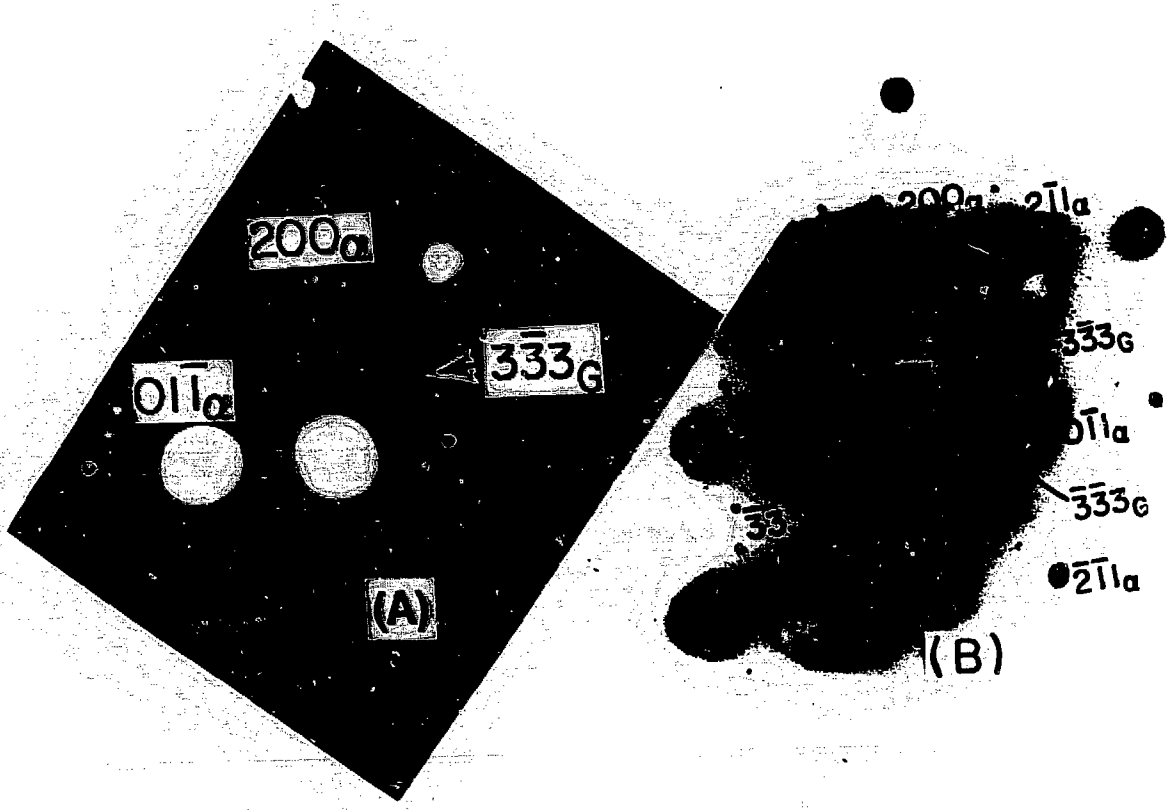

Fig. 3. Comparison of SAD Patterns Showing that the Type-X and G-Phase Reflections are Identical. (A) SAD pattern from a region containing small amounts of Type-X precipitates on dislocations which show only two reflections of the precipitate and (B) SAD pattern from a region containing a large amount of G-phase after aging at 400°C for 66,650 h. Only strong $(3\bar{3}3)_G$ and $(\bar{3}3\bar{3})_G$ reflections of the G-phase are present in (A).

corresponding to the α' phase, i.e., precipitates of ~1.5 nm or less in size. For the SANS experiment, the minimum distance between the specimen and detector was ~2 m. This would limit the maximum angle of detection of the scattering neutrons, and hence, the α' precipitates of very fine size that would scatter neutrons in large angles may not have been detected.

Several specimens aged under different conditions were analyzed by APFIM and the results were compared with TEM observations to evaluate the precipitation behavior. The results of the APFIM analysis have been reported elsewhere.[16,17] This technique is ideally suited for obtaining local chemical compositions over a very fine scale. The concentration profiles for Cr, Fe, and Ni in the ferrite phase of GF heat that was aged for 70,000 h at 300°C and the material from the KRB pump cover plate are shown in Figs. 4 and 5, respectively. The Cr-rich regions show a relative depletion of Fe and Ni, and vice versa. This one-to-one correspondence between Cr enrichment and Fe and Ni depletion indicates that the elemental fluctuations are not random but produced as a result of spinodal decomposition similar to that of the binary Fe-Cr ferritic alloy.[18] The thickness of the Cr-rich regions is estimated to be ~1.5 nm and the spacing between these regions ~5 to 6 nm. This is in good agreement with the characteristic mottled images of α' phase, obtained by TEM techniques (Fig. 4b).

The concentration profiles for the KRB pump cover material are comparable to those of the GF heat aged at 300°C for ~8 yr. In contrast to the Cr segregation profiles of the specimens aged at 300°C, the Cr profile developed during the 400°C aging showed more regular spacing between the Cr-depleted regions. These results indicate that the extent of the spinodal decomposition is strongly influenced by temperature. However, the maximum Cr levels detected by the APFIM analyses are only ~50 at. %. This is in contrast to

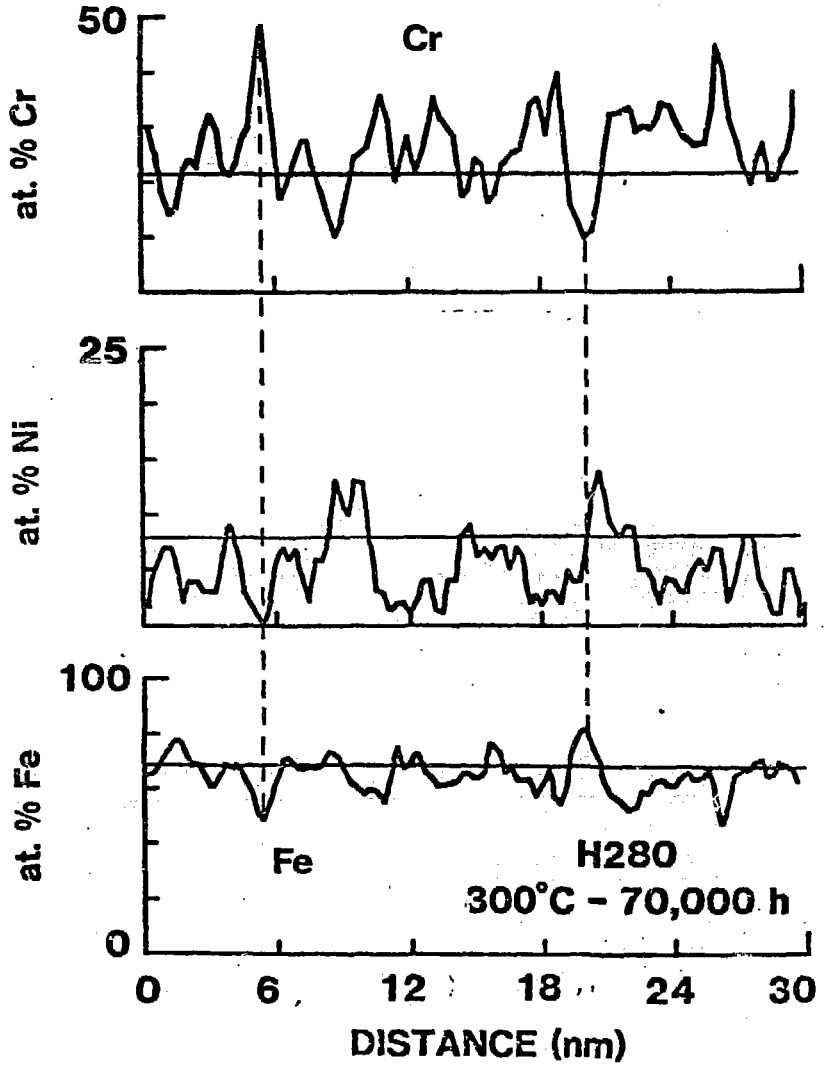

Fig. 4. Cr, Ni, and Fe Profiles in the Ferrite Phase of GF Heat 280 Specimen Aged at 300°C for 70,000 h (A), and Bright-Field TEM Image (B) Showing a Very Fine Scale Mottled Morphology Produced as a Result of the Fe and Cr Segregation.

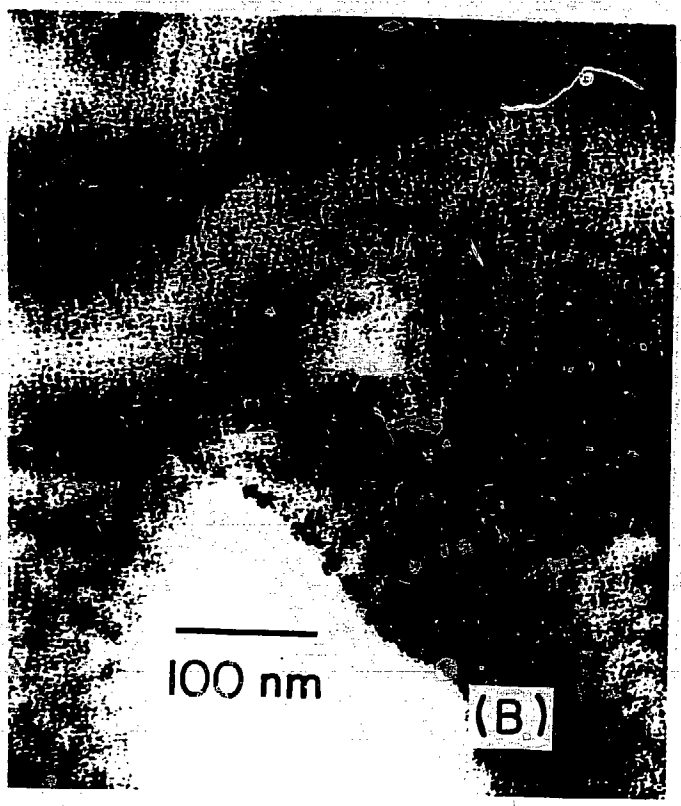

(B)

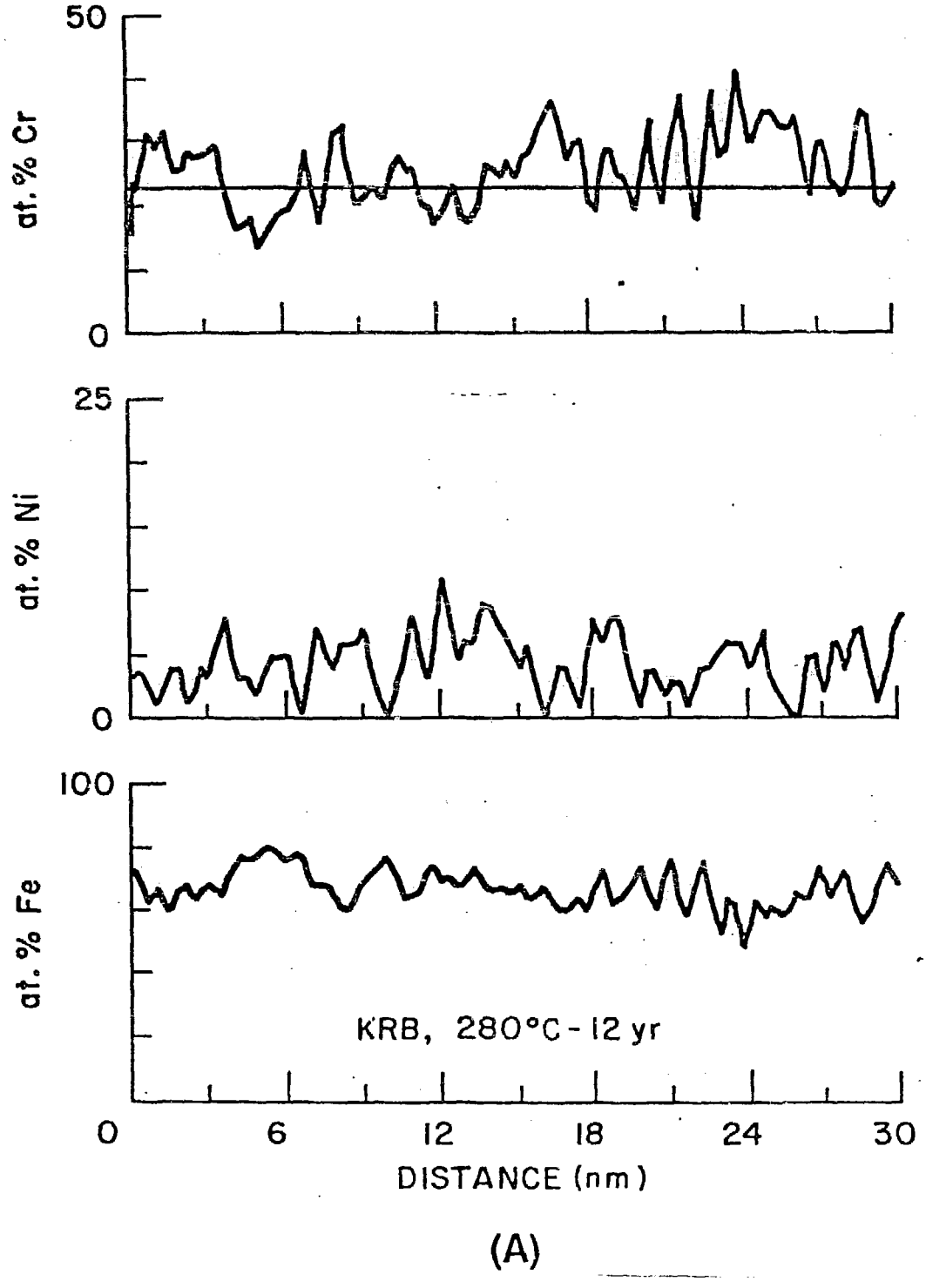

Fig. 5. Results Similar to Fig. 4 Obtained from KRB Boiling Water Reactor Pump Cover after a Nominal Service of 12 yr.

~78 at. % that has been reported for Fe-32 at. % Cr alloy.[18] Furthermore, for a given aging temperature, the maximum Cr level appears to be insensitive to aging time. These results indicate that the growth of the α' phase is very slow in the temperature range of the present investigation. It is possible that the spinodal decomposition and G-phase precipitation influence each other in cast duplex steel. The characteristics of the spinodal decomposition in the ferrite phase of the duplex structure may also be somewhat different from those of the binary ferritic alloy. The mechanical property data obtained from the accelerated aging at $\geq$400°C cannot be extrapolated to 300°C aging without a proper understanding of the possible interactions between the spinodal decomposition and the G-phase precipitation.

4. Charpy-impact Tests

Charpy-impact tests were completed at room temperature on thermally aged material from 11 small experimental heats and 5 commercial heats. The material was aged up to 10,000 h at 450, 400, and 350°C. Standard Charpy V-notch specimens were machined from the aged and unaged materials according to ASTM specification E-23. A Dynatup Model 8000A drop weight impact machine with an instrumented tup and data-readout system was used for the tests. The data for some of the heats are presented in Figs. 6-8. The different temperatures and times for aging were normalized in terms of the parameter P, which is determined from Eqs. (1) and (2). The significant results are as follows:

a. For all grades of cast material, the extent of embrittlement increases with an increase in ferrite content.

b. The carbon content in the steel is an important factor in controlling the overall process of embrittlement. The low-

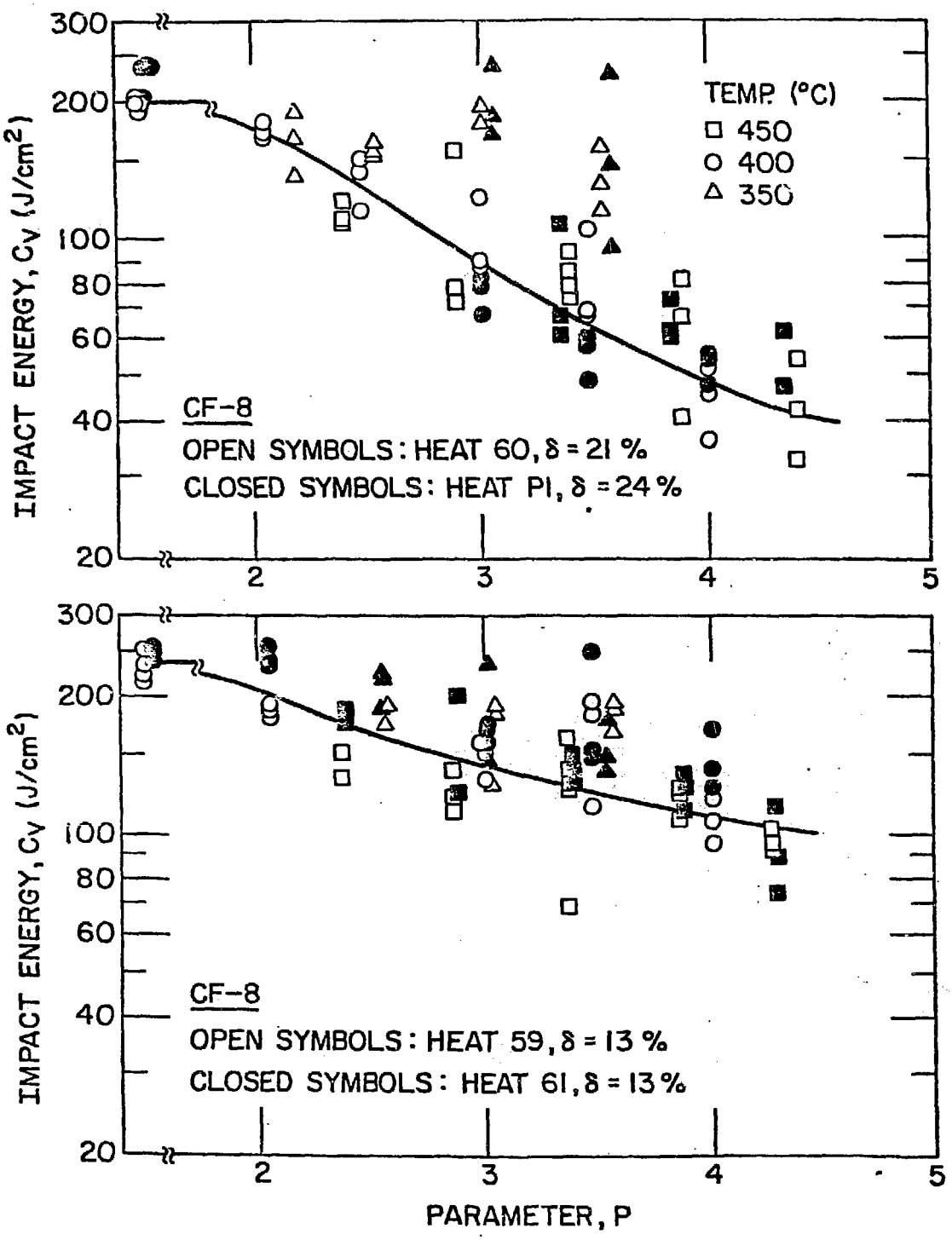

Fig. 6. Influence of Thermal Aging on the Room-temperature Impact Energy of CF-8 Cast Stainless Steel.

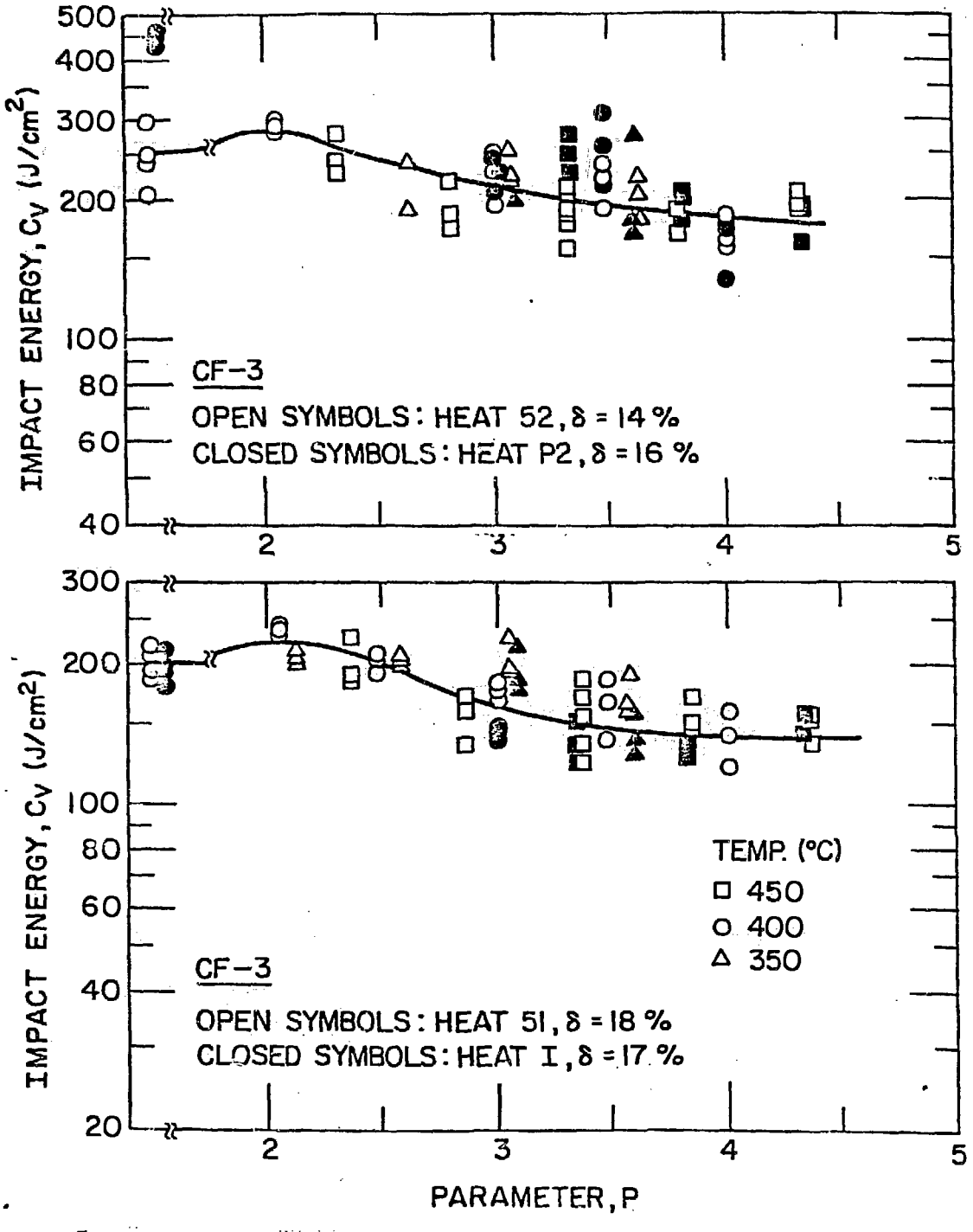

Fig. 7. Influence of Thermal Aging on the Room-temperature Impact Energy of CF-3 Cast Stainless Steel.

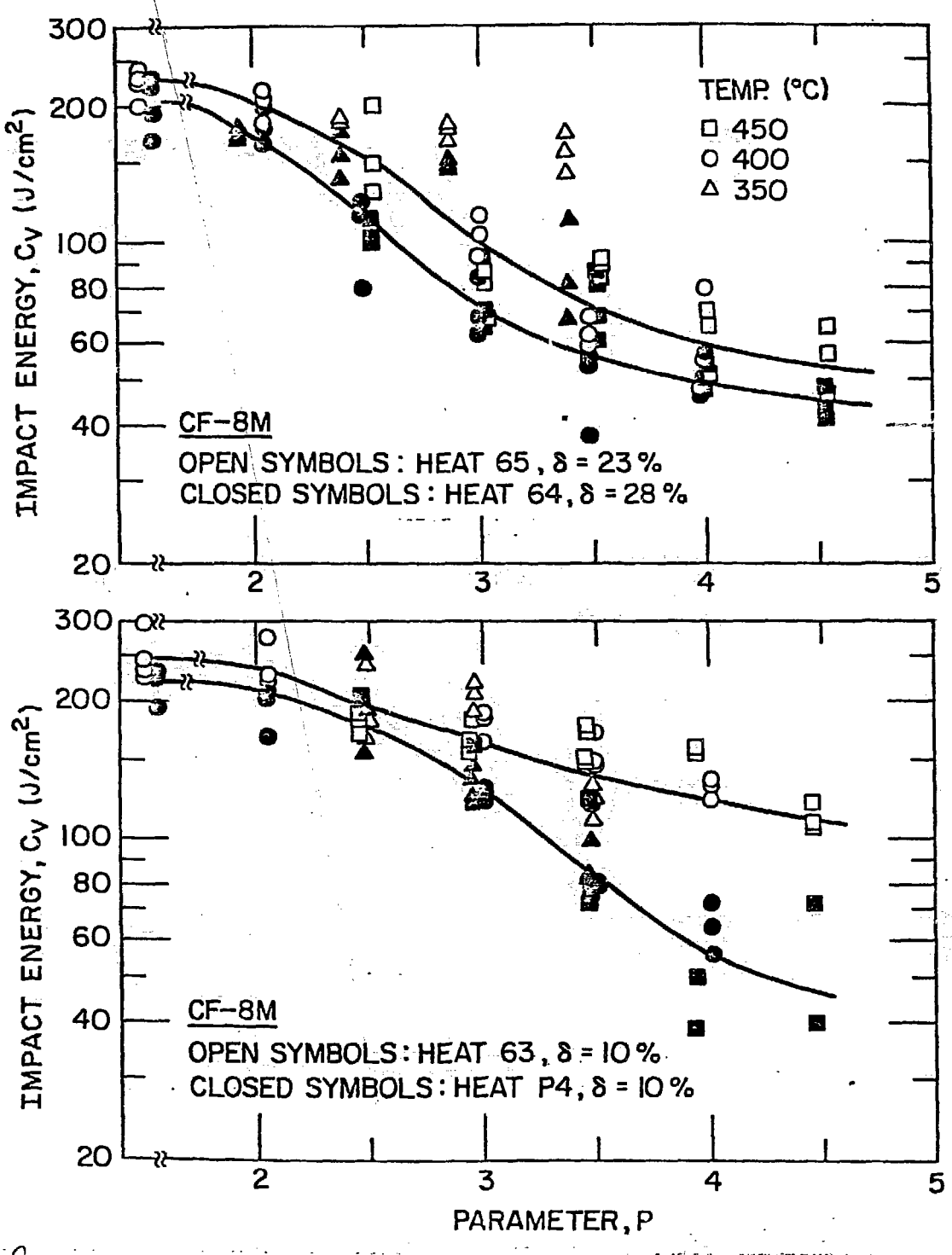

Fig. 8. Influence of Thermal Aging on the Room-temperature Impact Energy of CF-8M Cast Stainless Steel.

carbon CF-3 grade of cast steels is more resistant to embrittlement than the high-carbon CF-8 or CF-8M grade of materials. For example, after aging for 10,000 h at 400°C ($P \simeq 4$), the impact energy of heats I, 51, and 52 (CF-3 grade with 14 to 18% ferrite) decreases by ~30%, whereas heats 59 and 61 (CF-8 grade with 13% ferrite) or heat 63 (CF-8M grade with 10% ferrite) show ~50% reduction in impact energy.

c. Materials from heats 63 and P4 of CF-8M steel with 10% ferrite show significantly different embrittlement behavior, e.g., the impact energy after aging at 400°C for 9980 h decreases by 48% for heat 63 and 71% for heat P4 (Fig. 8). The latter has higher nitrogen content (0.153 wt % N) and a larger mean ferrite intercept distance (184 μm). Both of these factors probably influence the embrittlement behavior.

d. The impact data for CF-8 and -8M materials aged at different temperatures do not show a unique dependence on the aging parameter P. The onset of embrittlement is sooner for materials aged at 450 or 400°C than for those aged at 350°C (Figs. 6 and 8). These results indicate that the activation energies obtained from Eq. (2) do not accurately represent the embrittlement behavior of high-carbon grades of cast stainless steel over the temperature range of 300 to 450°C.

The data on microstructural characterization, presented in the previous section, indicate that at least two processes contribute to the embrittlement

of cast duplex stainless steel, viz., the embrittlement of ferrite matrix by the formation of α' and G phases and weakening of the ferrite/austenite phase boundary by carbide precipitation. The former occurs in all heats of cast stainless steel and is primarily responsible for their low-temperature embrittlement, whereas the precipitation of $M_{23}C_6$ carbides at the ferrite/austenite phase boundaries is important for embrittlement of the high-carbon grades of cast stainless steel.

Charpy-impact tests were conducted at liquid nitrogen temperature (i.e., -196°C) to assess the relative contributions of embrittlement of the ferrite matrix and phase boundary weakening to the loss of toughness and to help characterize the metallurgical parameters which influence fracture toughness. The fracture surfaces of the impact specimens were examined by SEM to determine the fracture mode. The Charpy-impact data for unaged and aged material tested at -196°C and at room temperature are given in Table 1. The results indicate that carbides are present in the as-cast structure of the high-carbon CF-8 steels. For the same ferrite content, the impact energies for the unaged CF-3 and -8M steels are about the same, but significantly higher than for unaged CF-8 steels. The fracture surfaces of the latter show cleavage of ferrite phase as well as separation of ferrite/austenite phase boundaries. The lower impact energy for CF-8 steels is due to the presence of phase boundary carbides which precipitate during the water quenching treatment for the casting. Such carbides do not form in the low-carbon CF-3 steels, and the Mo-containing CF-8M steels are inherently tougher because the carbides precipitate in the ferrite matrix rather than at the phase boundaries.

For each grade of unaged cast steel, the impact energy at -196°C decreases with an increase in ferrite content. At this temperature, the ferrite phase is brittle; consequently, the impact strength of the duplex

TABLE 1. Charpy-impact Data for Cast Duplex Stainless Steel

Heat	Ferrite Content, %	Grade	Charpy V-Notch Impact Energy, J/cm^2					
			Unaged		Aged 10^4 h at 400°C		Aged 10^4 h at 450°C	
			-196°C	25°C	-196°C	25°C	-196°C	25°C
57	4.0	CF-8	119	223	-	-	-	-
53	8.7		83	234	-	-	-	-
56	10.1		88	206	-	148	-	109
59	13.5		53	228	14	107	14	97
61	13.1		42	250	-	145	-	93
60	21.1		24	197	8	56	10	43
P1[a]	24.1		44	221	9	52	-	56
49	7.2	CF-3	190	228	-	-	-	-
48	8.7		186	226	-	-	-	-
52	13.5		151	248	37	168	138	198
P2[a]	15.6		178	401	43	159	-	182
47	16.3		133	229	-	168	-	-
I[a]	17.1		170	194	49	156	-	153
51	18.0		139	201	36	140	67	151
62	4.4	CF-8M	188	228	-	-	-	-
63	10.4		198	250	42	130	32	112
P4[a]	10.4		34	227	-	65	-	57
66	19.9		155	221	16	106	26	107
65	23.4		80	223	-	62	-	57
64	28.4		82	201	10	52	8	45

[a]Commercial heats.

steel will decrease with an increase in ferrite content. The unaged material from heat P4 (CF-8M grade) shows a very low impact energy at -196°C. The fracture surfaces of the Charpy specimens show phase-boundarty separation as well as cleavage of the ferrite phase. This heat has a high nitrogen content. The low impact energy of the unaged material is probably due to the presence of nitrides and possibly carbides in the as-cast material.

The data on aged material show that additional precipitation of phase boundary carbides and/or growth of existing carbides occurs in the high-carbon CF-8 and -8M steels during aging at 400 or 450°C. The impact energy of the aged material tested at -196 or 25°C is significantly lower than that of the unaged material. The aged CF-3 steels also show appreciable reduction in impact energy, particularly at -196°C. Metallographic results indicate that the decrease in impact energy for the CF-3 steels and the CF-8 or -8M steels is caused by different processes. The fracture surfaces of impact specimens of heat 51 (CF-3 grade) and 60 (CF-8 grade) tested at -196°C are shown in Figs. 9 and 10, respectively. Although heat 51 contains 18% ferrite, the fracture occurs primarily by cleavage of the ferrite phase. The fracture surface of unaged specimen of heat 51 contains some ductile failure of austenite phase. In contrast, the fracture surfaces of heat 60 show cleavage of ferrite phase as well as phase boundary separation (e.g., regions marked S in Fig. 10). The fracture mode for specimens aged for 9980 h at 450°C is predominantly phase boundary separation. These results indicate that the reduction in impact strength of aged CF-3 steels is caused by embrittlement of ferrite matrix by precipitate phases, while embrittlement of ferrite matrix as well as the weakening of phase boundary by carbides cause degradation of the high-carbon CF-8 and -8M steels.[8,11]

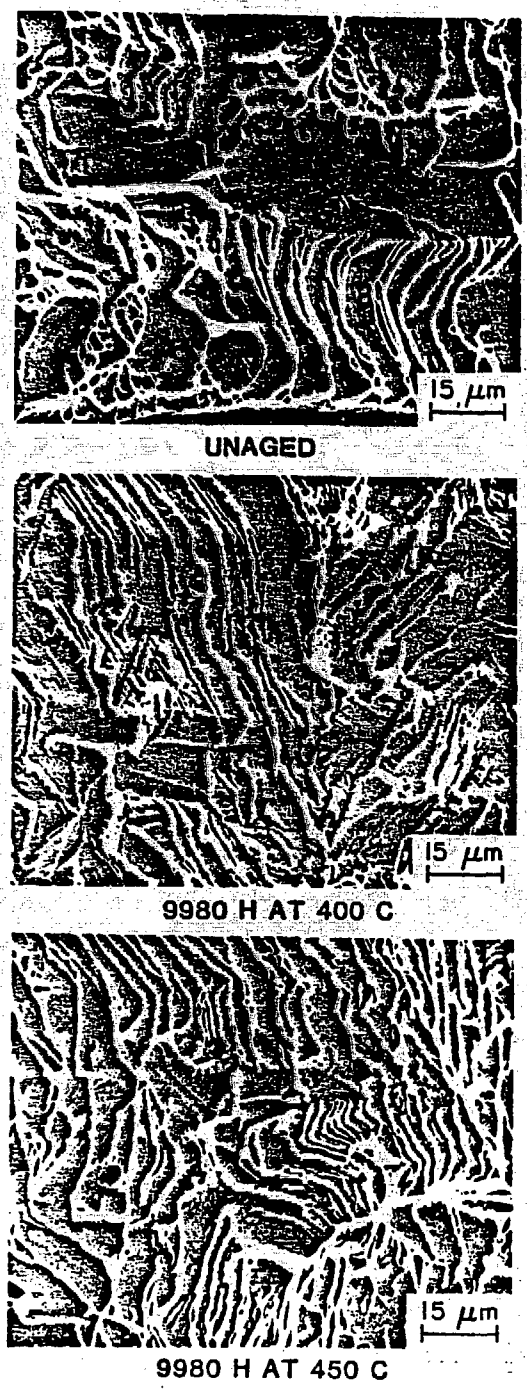

Fig. 9. Fracture Surfaces of Impact Test Specimens of Unaged and Aged CF-3 Cast Steel (Heat 51, 18% Ferrite) Tested at -196°C.

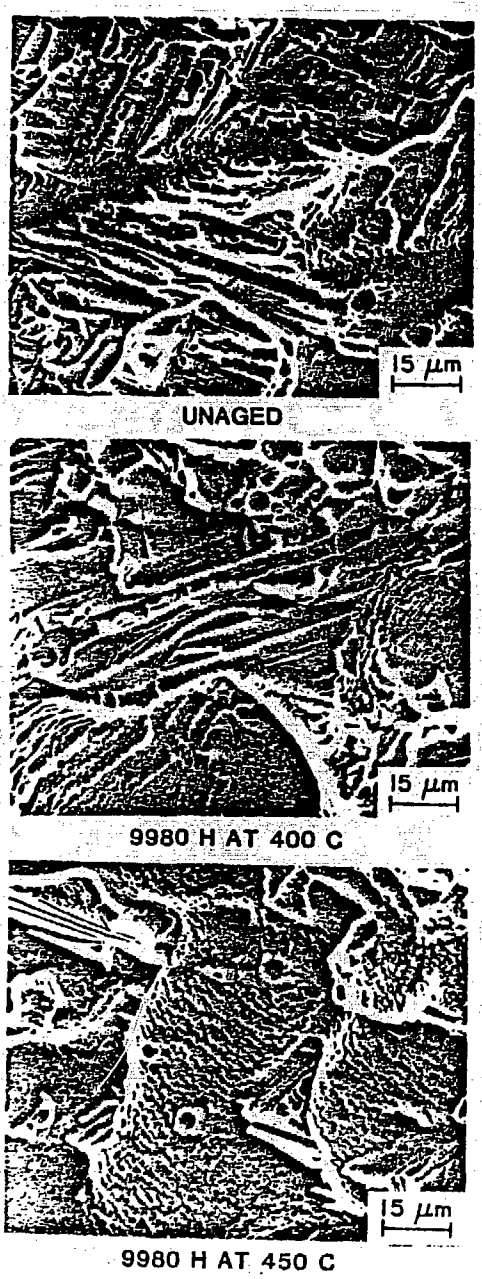

Fig. 10. Fracture Surfaces of Impact Test Specimens of Unaged and Aged CF-8 Cast Steel (Heat 60, 21% Ferrite) Tested at -196°C.

The data for aged material indicate that the impact energy for CF-3 specimens aged at 450°C is higher than those aged at 400°C for the same time. This behavior is quite pronounced for tests at -196°C. These results suggest that the precipitation of α' and G phases is strongly dependent on temperature. The differences in impact energy for material aged at different temperatures may be attributed to the relative contributions of α' and G phases to the overall process of embrittlement.

The differences in the mechanism of embrittlement are reflected in the load-time curves obtained for the impact tests on different heats of material. The load-time curves for unaged and aged specimens of heats 51 (CF-3 steel) and 60 (CF-8 steel) tested at -196°C are shown in Fig. 11. Specimens from heat 51 exhibit a typical load-time curve with a gradual decrease in load during fracture. The thermally aged materials show a decrease in impact energy (represented by the area under the curve) and a higher strain hardening rate, due to the precipitation of additional phases in the ferrite matrix. However, the impact energy for the specimen aged at 450°C is greater than for the specimen aged at 400°C. Since the low-carbon CF-3 steel is free from phase boundary carbides, these results suggest differences in the precipitation behavior in the ferrite matrix. The load-time curves for heat 60 (CF-8 steel) show very little deformation and a sudden drop in load just past the yield point. The maximum load for these specimens is significantly lower than for the specimens from heat 51. The fracture surfaces of the impact specimens show predominantly phase boundary separation. These results indicate that the sudden drop in load is associated with phase boundary separation.

Charpy-impact tests were conducted at temperatures between -196 and 290°C on two commercial heats of CF-3 stainless steel to determine the effect of

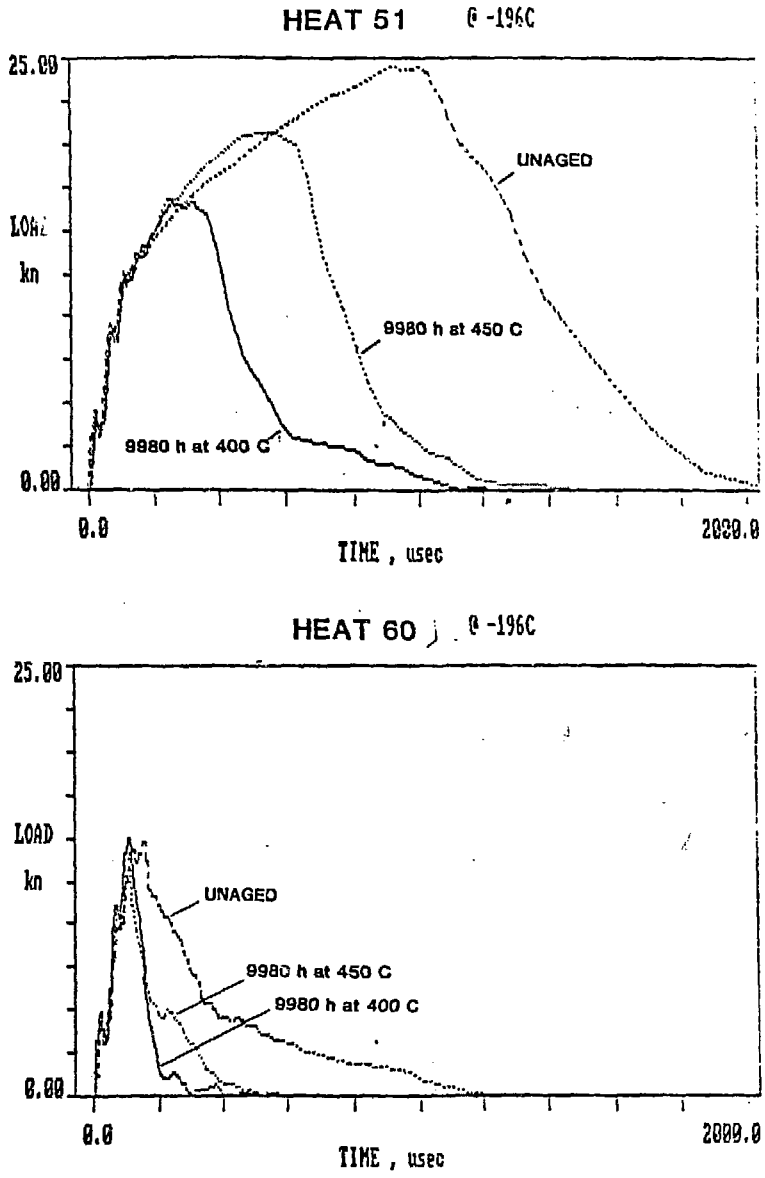

Fig. 22. Load-Time Curves for Charpy V-Notch Specimens of Heats 51 and 60 Tested at -196°C.

aging on ductile-to-brittle transition temperature (DBTT). The results for unaged and aged materials from the static cast pump impeller (heat I) and a centrifugally cast pipe (heat P2) are shown in Fig. 12. Specimens from the pipe material were in the L-C as well as C-L orientation.* Although both heats contain approximately the same amount of ferrite, the DBTT curves for the two steels are significantly different, viz., at temperatures greater than -100°C the impact strength of heat P2 is a factor of two greater than that for heat I. Furthermore, the impact energy of heat I shows little change with tempeature and the DBTT curve is nearly flat. Such differences arise from differences in the initial heat treatment, section thickness, and casting conditions, which influence the macrostructure of the steel. The low-carbon CF-3 steels do not contain phase-boundary carbides and exhibit high impact strength at low temperatures, e.g., the impact energy of heats P2 and I at -196°C is $\geq$150 J/cm^2 as compared to <50 J/cm^2 for the CF-8 stainless steels. The results for aged material indicate that thermal aging decreases the impact energy of these steels. However, the shift in DBTT curves is significantly different for the two steels, namely, heat I shows a decrease in impact energy at all temperatures, whereas, heat P2 shows large reductions in impact energy only at temperatures <50°C. Impact tests are in progress on six experimental heats and on material aged for longer times to determine the influence of compositional and metallurgical variables on DBTT curves.

The DBTT curve for material from the KRB pump cover plate is shown in Fig. 13. The material was at the service temperature for ~8 yr. Data obtained by Georg Fischer Co. on Charpy U-notch specimens are also included in

*L - longitudinal or axial direction and C - circumferential direction. The first digit designates the direction normal to the crack plane and second digit the direction of crack propagation.

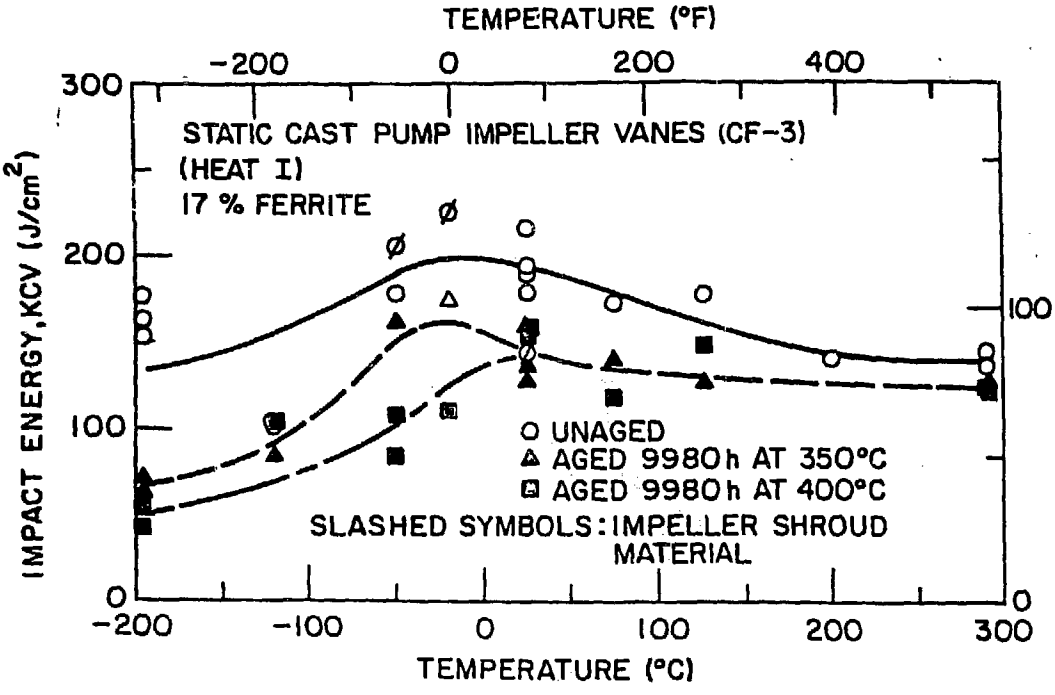

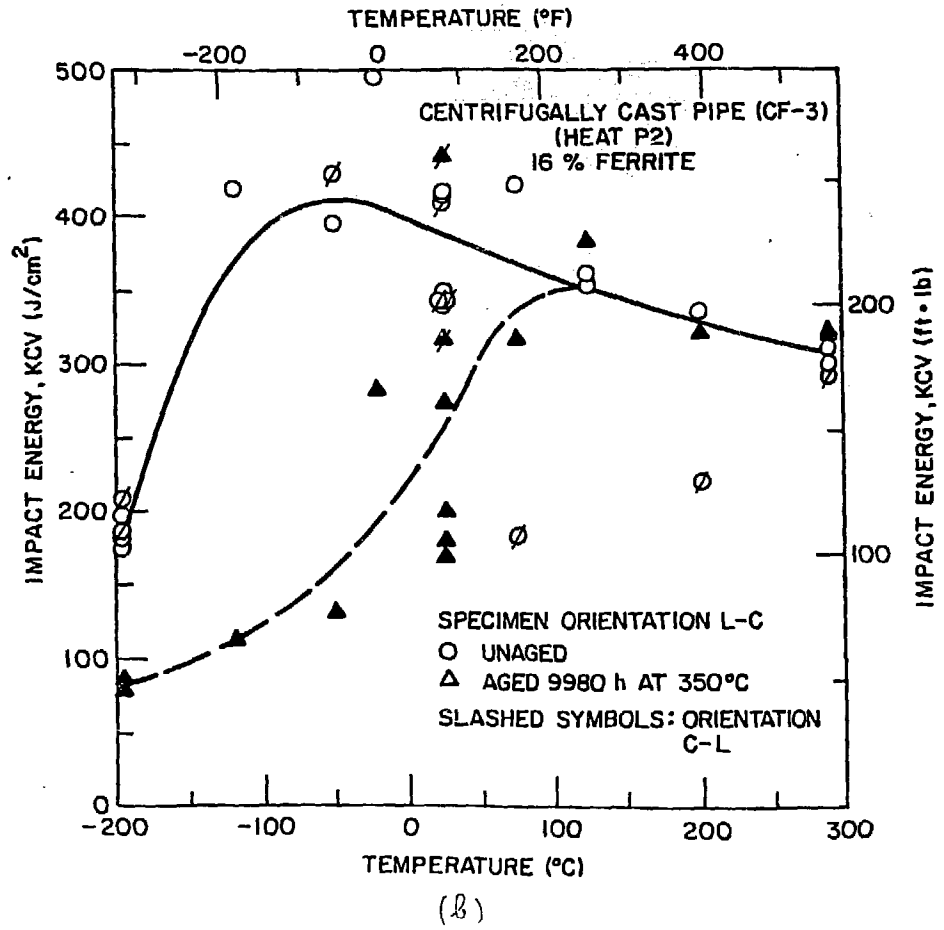

Fig. 12. Influence of Test Temperature on Charpy V-Notch Impact Energy for Unaged and Aged Material from (a) Heat I and (b) Heat P2.

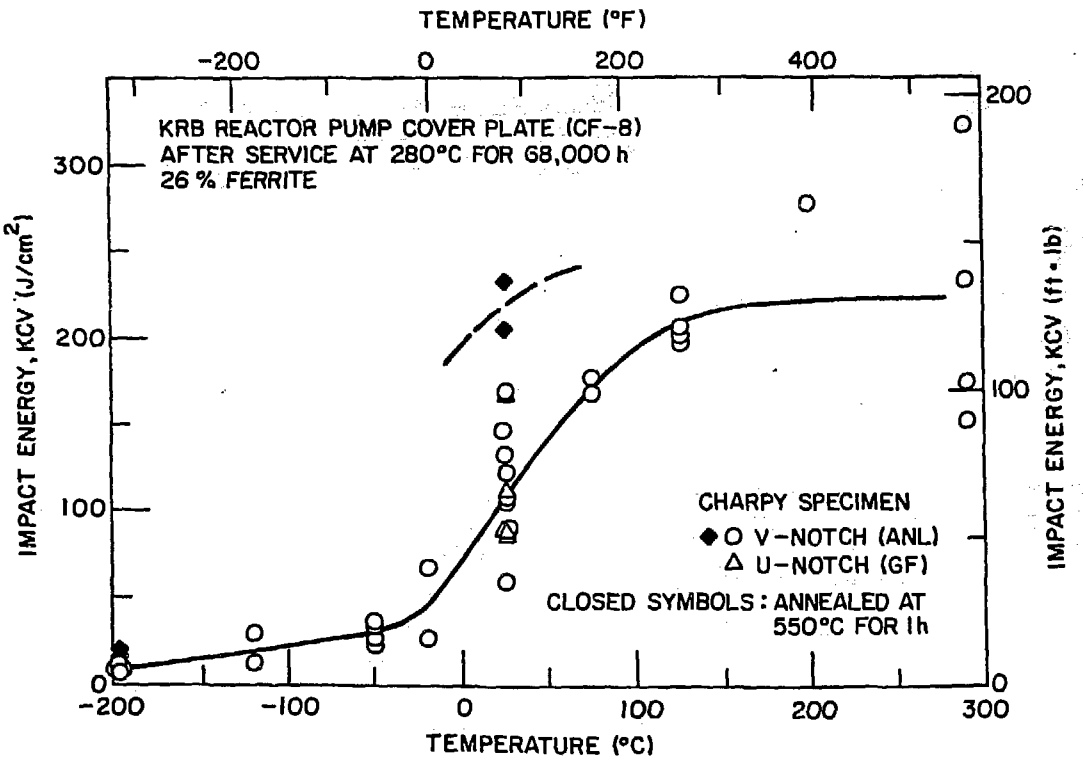

Fig. 13. Influence of Test Temperature on Charpy V-Notch Impact Energy for the KRB Reactor Pump Cover Plate Material.

the figure. The U-notch impact energies were converted to KCV values using a correlation developed by FRAMATOM.[19] The upper- and lower-shelf values for the material are 220 ± 75 and 10 ± 2 J/cm^2 (130 and 6 ft lb), respectively. The lower shelf value is small because of the presence of phase boundary carbides. The fracture surfaces of the specimens tested at low temperatures (i.e., less than 25°C) show cleavage of the ferrite phase as well as phase boundary separation.

Scoping tests were conducted to investigate the possibility of recovering the loss in fracture toughness of low-temperature-aged cast stainless steel. Tests on ferritic and martensitic steels have shown that the loss of toughness of low-temperature-aged materials can be recovered by a short-term anneal at 550°C.[20] The time-temperature-transformation curves for binary Fe-Cr alloys indicate that the α' phase is not stable at 550°C. However, these alloys are embrittled after aging for >10 h at 550°C due to the formation of sigma phase. Consequently, the low-temperature-aged materials were aged for ~1 h at 550°C to dissolve the α' phase and yet avoid the formation of sigma phase. The impact energies for the KRB pump cover plate material, which was given the above heat treatment, are shown in Fig. 13. The impact energies at room temperature and at -196°C increased from 113 ± 33 and 10 ± 2 J/cm^2 to 223 ± 13 and 17 ± 1 J/cm^2, respectively. Material from ANL heat 60 (CF-8 steel) aged for 9980 h at 400°C was also annealed for 1 h at 550°C. The microhardness of the ferrite phase decreased from 377 to 246 VHN. The microhardness of the ferrite in the unaged material was 260 VHN. TEM examination of the specimens is in progress to characterize the microstructure and to determine the role of G-phase in low-temperature embrittlement of cast stainless steel.

5. Tensile and J-R Curve Tests

Tensile and J-R curve tests have been completed at Materials Engineering Associates, Inc. (MEA) on three commercial heats which were aged up to 10,000 h at 350 and 400°C. Tensile tests were performed on cylinidrical specimens with a diameter and gauge length of 5.1 and 18.5 mm, respectively, in accordance with ASTM specifications E8 and E21. The specimens were machined along the axial as well as circumferential directions of the cast pipes (heats P1 and P2) and the shroud of the pump impeller (heat I). The J-R curve tests were conducted on 1-T compact tension (CT) specimens in accordance with ASTM specification E813. The V-notch for the CT specimens was in the L-C and C-L orientations.

The tensile properties of unaged and aged cast stainless steel at room temperature and at 288°C are given in Table 2. The results indicate that at both temperatures, thermal aging of the material results in an increase in both yield and ultimate stress and a slight decrease in ductility. The change in tensile properties is larger for the material aged at higher temperature, i.e., at 400°C. For the three heats tested, orientation has little or no effect, i.e., the properties in the axial and circumferential directions of the castings are comparable.

The results for J-R curve tests indicate that thermal aging decreases the J_{IC} as well as the tearing modulus of the cast material. The reduction in fracture toughness is greater for materials aged for 9980 h at 400°C than those aged at 350°C for similar times. Typical crack growth fracture resistance curves for heat P1 at room temperature and 288°C are given in Fig. 14. The fracture toughness results show good agreement with the Charpy-impact data, i.e., unaged and aged materials which show high impact strength also exhibit greater fracture toughness. The J_{IC} values and Charpy V-notch

TABLE 2. Tensile Properties of Unaged and Aged Cast Stainless Steel at Room Temperature and at 288°C

Heat	Aging Condition Temp., °C	Aging Condition Time, h	0.2% Yield Stress, MPa Axial	0.2% Yield Stress, MPa Circum.	Ultimate Stress, MPa Axial	Ultimate Stress, MPa Circum.	Reduction in Area, % Axial	Reduction in Area, % Circum.
				Room Temperature				
P1	-	-	247	244 ± 2	582 ± 4	583 ± 3	66 ± 8	66 ± 2
	350	9980	281 ± 14	270 ± 9	635 ± 25	609 ± 1	78 ± 4	68 ± 12
	400	9980	286	285	677	660	56	56
P2	-	-	213 ± 8	230 ± 21	550 ± 18	548 ± 13	80 ± 4	80 ± 5
	350	3000	249	252	594	602	89	85
	350	9980	265	-	609	-	78	-
	400	9980	236	234	617	603	78	69
I	-	-	254 ± 10	-	585 ± 9	-	78 ± 3	-
	350	9980	300 ± 17	-	634 ± 16	-	69 ± 8	-
				288°C				
P1	-	-	157 ± 4	153 ± 5	434 ± 13	424 ± 21	70 ± 16	63 ± 5
	350	9980	177 ± 5	180	455 ± 5	454	59 ± 5	63
	400	9980	163	167	486	502	51	50
P2	-	-	141 ± 3	160 ± 7	396 ± 15	396 ± 13	71 ± 2	82 ± 9
	350	3000	161	154	415	399	80	67
	350	9980	154	156	419	424	73	71
	400	9980	147	160	431	447	54	56
I	-	-	174 ± 7	-	406 ± 5	-	62 ± 4	-
	350	9980	187 ± 7	-	421 ± 34	-	49 ± 12	-

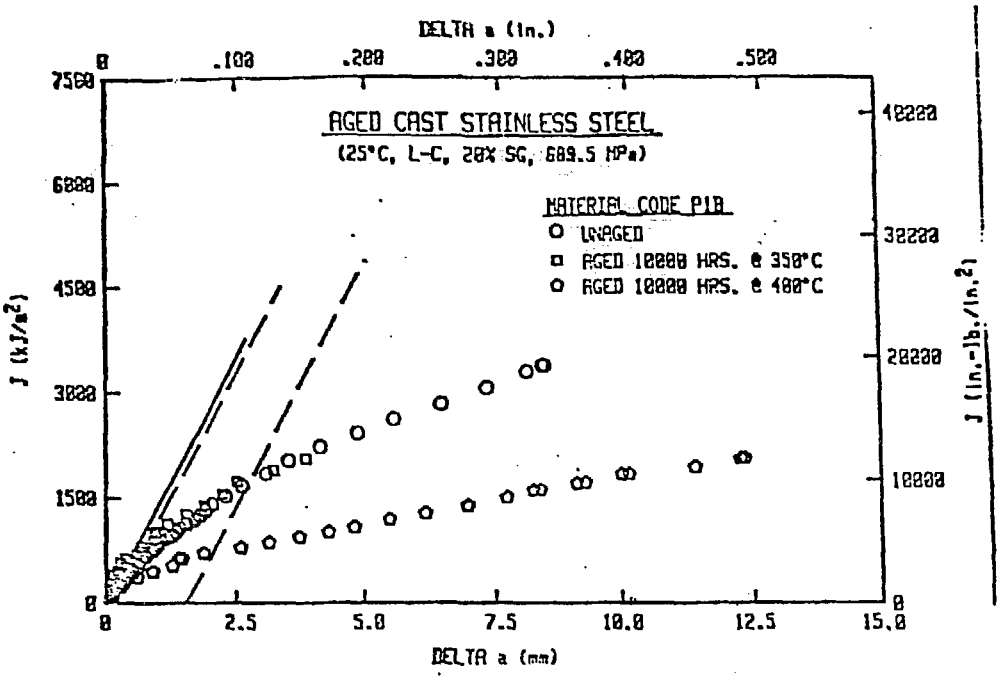

(a)

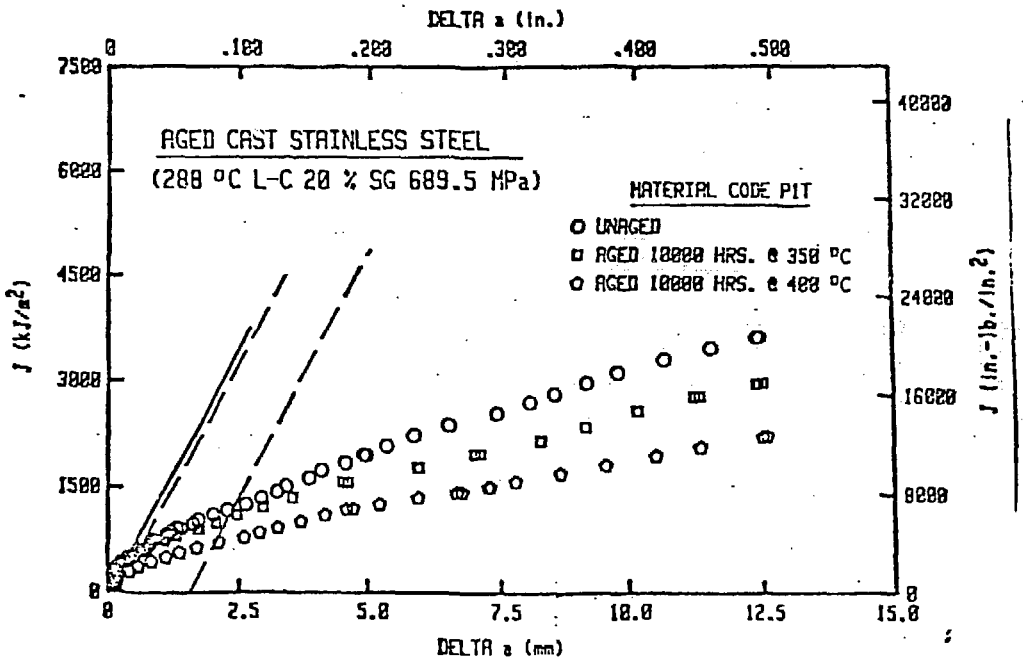

(b)

Fig. 14. Crack Growth Fracture Resistance Behavior of Thermally Aged CF-8 Cast Stainless Steel at (a) Room Temperature and (b) 288°C.

impact energies obtained at room temperature for the various materials are plotted in Fig. 15. After aging for 9980 h at 400°C, the J_{IC} value for heat P1 (CF-8 steel) at room temperature decreased from 2171 to 254 kJ/m^2 and the tearing modulus decreased from 546 to 200. The fracture toughness of the low-carbon CF-3 steels (i.e., heats P2 and I) was higher.

Tensile and J-R curve tests are in progress on six experimental heats that were aged up to 10,000 h at 320, 350, 400, and 450°C. The fracture toughness results will be correlated with Charpy-impact data to determine the effects of metallurgical variables on fracture toughness and establish the extent of embrittlement expected during the service life of reactor components.

6. Conclusions

The results from microstructural characterization of long-term aged materials by APFIM and TEM techniques indicate that formation of α' precipitates by spinodal decomposition is the primary mechanism of in-reactor aging embrittlement of cast duplex stainless steel. In contrast, the G-phase precipitation, which is primarily limited to dislocations at ~300°C, appears to be a secondary mechanism. It is not clear, however, whether the interactions between the spinodal decomposition and G-phase precipitation change with aging temperature and, therefore, influence the kinetics of the process of embrittlement. TEM analyses show that the precipitates, designated as Type-X phase in earlier reports, are, in fact, the G-phase which form preferentially on dislocations during aging at low temperatures (i.e., ~300°C). Microstructural data also indicate that weakening of the ferrite/austenite phase boundary by carbide precipitates has a significant effect on the onset and extent of embrittlement of the high-carbon CF-8 and CF-8M grades of stainless steels. These results suggest that extrapolation of

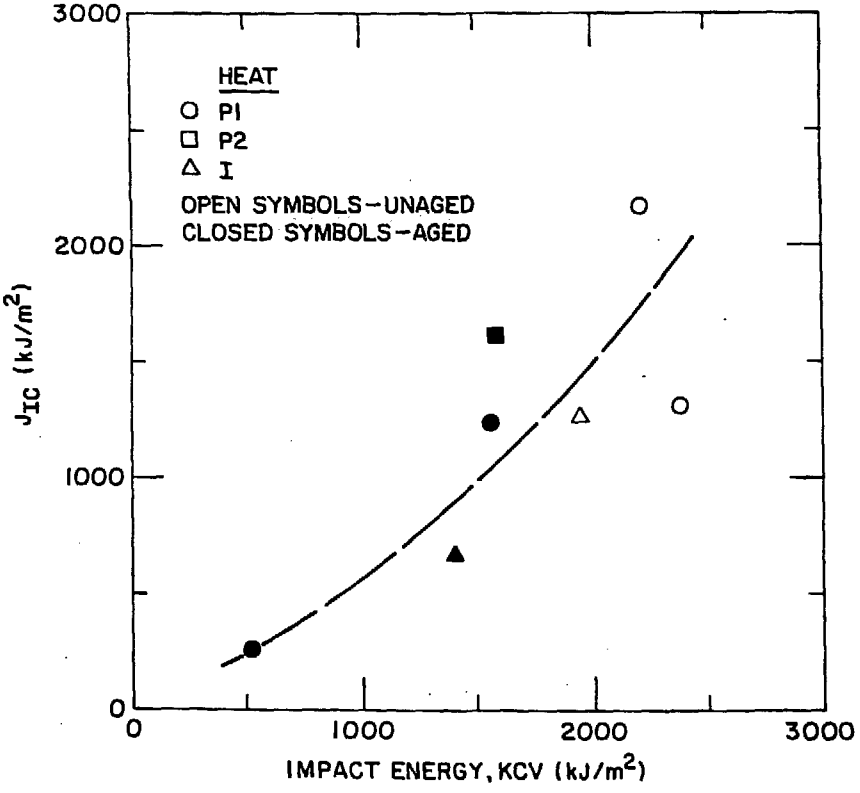

Fig. 15. Correlation Between J_{IC} and Impact Energy for Cast Duplex Stainless Steel.

high-temperature laboratory data (i.e., at temperatures $\geq$400°C) to reactor temperatures may not be valid for the high-carbon grades of cast stainless steel. For the low-carbon CF-3 steels, extrapolation of laboratory data to reactor conditions requires a proper understanding of the possible interaction between the spinodal decomposition and G-phase precipitation.

Mechanical property data from Charpy-impact, tensile, and J-R curve tests indicate that the ferrite content, concentrations of C and N in the steel, and possibly the ferrite morphology are important factors in controlling low-temperature embrittlement of cast stainless steel. Thermal aging of cast materials increases the tensile strength while the impact energy, J_{IC}, and tearing modulus are decreased. The J_{IC} values show good agreement with the Charpy-impact data, i.e., materials with low impact energy show small fracture toughness. For example, aging at 400°C for 9980 h of a CF-8 material with 24% ferrite (i.e., heat P1), decreased the room-temperature impact energy from ~220 to 50 J/cm^2 and the J_{IC} values decreased from ~2170 to 250 kJ/m^2. The tearing modulus of the aged material was relatively high, viz., the tearing modulus at room temperature decreased from ~550 to 200. In general, the high-carbon CF-8 and CF-8M grades of cast steels show lower toughness than the low-carbon CF-3 grades, due to the weakening of the phase boundaries by carbide precipitates.

Acknowledgments

The authors acknowledge the experimental contributions provided by A. Sather and W. K. Soppet and microscopic assistance received from R. A. Conner, Jr. and G. M. Dragel. This work was supported by the Office of Nuclear Regulatory Research, U. S. Nuclear Regulatory Commission, under Contract W-31-109-Eng-38.

References

1. H. D. Solomon and T. M. Devine, "Influence of Microstructure on the Mechanical Properties and Localized Corrosion of a Duplex Stainless Steel," in Micon 78: Optimization of Processing, Properties, and Service Performance through Microstructural Control, eds. Abrams, Maniar, Nail, and Solomon, ASTM STP 672 (1979), p. 430.

2. P. J. Grobner, "The 885°F (475°C) Embrittlement of Ferritic Stainless Steels," Metall. Trans. 4 (1973), p. 251.

3. T. J. Nichol, A. Datta, and G. Aggen, "Embrittlement of Ferritic Stainless Steels," Metall. Trans. 11A (1980), p. 573.

4. A. Trautwein and W. Gysel, "Influence of Long Time Aging of CF-8 and CF-8M Cast Steel at Temperatures Between 300 and 500 deg. C on the Impact Toughness and the Structure Properties," Spectrum, Technische Mitteilungen aus dem GF Konzern, No. 5 (May 1981); Stainless Steel Castings, eds. V. G. Behal and A. S. Melilli, ASTM STM 756 (1982), p. 165.

5. G. Baudry and C. Pichard, "Evolution During Long Holding Times at 300 and 450°C of the Mechanical Properties of Austeno-Ferritic Steel Castings and Welded Joints Used in Pressurized Water Nuclear Reactors," in Troisieme Congres National Sur La Technologie Des Appareils a Bression, Vol. 2, Materiaux, A.F.I.A.P. (1980), p. 673.

6. E. I. Landerman and W. H. Bamford, "Fracture Toughness and Fatigue Characteristics of Centrifugally Cast Type 316 Stainless Steel Pipe after Simulated Thermal Service Conditions, Ductility, and Toughness Considerations in Elevated Temperature Service," ASME MPC-8 (1978), p. 99.

7. G. Slama, P. Petrequin, and T. Magep, "Effect of Aging on Mechanical Properties of Austenitic Stainless Steel Castings and Welds," presented at SMIRT Post-Conference Seminar 6, Assuring Structural Integrity of Steel Reactor Pressure Boundary Components, August 29 and 30, 1983, Monterey, CA.

8. O. K. Chopra and H. M. Chung, Long-Term Embrittlement of Cast Duplex Stainless Steels in LWR Systems: Annual Report, October 1984-September 1985, NUREG/CR-4503, ANL-86-3, Argonne National Laboratory.

9. O. K. Chopra and G. Ayrault, "Aging Degradation of Cast Stainless Steel: Status and Program," Nucl. Eng. Des. 86 (1985), p. 69.

10. O. K. Chopra and H. M. Chung, Long-Term Embrittlement of Cast Duplex Stainless Steels in LWR Systems: Annual Report, October 1983-September 1984, NUREG/CR-4204, ANL-85-20 (March 1985); Nucl. Eng. Des. 89 (1985), p. 305.

11. H. M. Chung and O. K. Chopra, "Microstructure of Cast Duplex Stainless Steel after Long-Term Aging," in Proc. Second Intl. Symp. on Environmental Degradation of Materials in Nuclear Power Systems - Water Reactors, September 9-12, 1985, Monterey, CA, American Nuclear Society, LaGrange Park, IL, pp. 287-292 (1986).

12. M. K. Miller, J. Bentley, S. S. Brenner, and J. A. Spitznagel, "Long Term Thermal Aging of Type CF-8 Stainless Steel," J. Phys. (Paris) Colloq. 45 (1984), p. C9-385.

13. J. Bentley, M. K. Miller, S. S. Brenner, and J. A. Spitznagel, "Identification of G-Phase in Aged Cast CF-8 Type Stainless Steel," Proc. 43rd Annual Meeting of the Electron Microscopy Society of America, G. W. Bailey, ed., San Francisco Press, 1985, pp. 328-329.

14. M. Vrinat, R. Cozar, and Y. Meyzaud, "Precipitated Phases in the Ferrite of Aged Cast Duplex Stainless Steel," Scripta Met. 20 (1986), p. 1101.

15. J. E. Epperson, J. S. Lin, and S. Spooner, "The Fine Scale Microstructure in Cast and Aged Duplex Stainless Steels Investigated by Small Angle Neutron Scattering," 13th Intl. Symp. on Effects of Radiation on Materials, June 23-25, 1986, Seattle, WA.

16. T. J. Godfrey and G. D. W. Smith, "The Atom Probe Analysis of a Cast Duplex Stainless Steel," 33rd Intl. Field Emission Symp., July 7-11, 1986, West Berlin, Germany.

17. M. K. Miller and J. Bentley, "Microstructural Characterization of Primary Coolant Pipe Steel," ibid.

18. S. S. Brenner, M. K. Miller, and W. A. Soffa, "Spinodal Decomposition of Iron-32 at. % Chromium at 470°C," Scripta Met. 16, 831-836 (1982).

19. Y. Meyzaud, Framatom, private communications.

20. A. Trautwein, Georg Fischer Co., private communications.